Nuclear Instruments and Methods in Physics Research B 283 (2012) 9–14

Contents lists available at SciVerse ScienceDirect

Nuclear Instruments and Methods in Physics Research B

journal homepage: www.elsevier.com/locate/nimb

Effects of 6 MeV electron irradiation on the electrical properties and device parameters of $Al/Al_2O_3/TiO_2/n$-Si MOS capacitors

P. Laha [a], I. Banerjee [a,1], P.K. Barhai [a], A.K. Das [b], V.N. Bhoraskar [c], S.K. Mahapatra [a,*]

[a] Department of Applied Physics, Birla Institute of Technology, Mesra, Ranchi 835215, India
[b] Laser & Plasma Technology Division, Bhabha Atomic Research Center, Mumbai 400085, India
[c] Department of Physics, University of Pune, Ganeshkhind, Pune 411007, India

ARTICLE INFO

Article history:
Received 22 December 2011
Received in revised form 2 April 2012
Available online 21 April 2012

Keywords:
Poole–Frenkel coefficient
Flat band voltage
Interface trap density
Surface charge density

ABSTRACT

The effects of 6 MeV electron irradiation on the electrical properties and device parameter characteristics of $Al/Al_2O_3/TiO_2/n$-Si metal–oxide–semiconductor capacitors have been studied. Twelve $Al/Al_2O_3/TiO_2/n$-Si MOS capacitors were fabricated using r.f. magnetron sputtering and divided into four groups. The first group was not irradiated and treated as virgin. The rest were irradiated with 6 MeV electrons at doses 10, 20, and 30 kGy, maintaining the dose rate at ~1 kGy/min. Variations in crystallinity of the virgin and irradiated capacitors were studied using grazing incident X-ray diffraction. The thickness and in-depth elemental distributions of individual layers were determined using secondary ion mass apectrometry. Capacitance–voltage, conductance–voltage and leakage current–voltage characteristics of the virgin and irradiated samples were studied. The device parameters (flat band voltage, surface charge density and interface trap density of the virgin and irradiated structures) were determined. The electrical properties of the capacitors were investigated and the Poole–Frenkel coefficient of the capacitors was determined from leakage current measurements. The leakage current mechanism has been explained.

© 2012 Elsevier B.V. All rights reserved.

1. Introduction

The space environment is complex and dynamic in nature. It consists of neutral species, charged particles, electric fields, magnetic fields, solar radiation, galactic radiation, space debris, etc. [1]. It leads to deterioration of the performance and lifetime of the MOS devices which are used in spacecraft [2,3]. In the last few decades, studies related to the design and characterization of MOS devices has been carried out to improve their performance [2]. The focus of several studies is on the dependence of MOS parameters on thickness, dielectric constant, grain size and crystallinity of the oxide materials [3] and also on the development of radiation hardened MOS devices using e-beam irradiation. Although the fabrication of the MOS device can be tailored by different methods to make it suitable for required applications the development of radiation hardened MOS device is still challenging [4]. The effect of ionizing radiation on MOS devices has been studied using e-beam irradiations [5]. The radiation induced defects, dangling bonds, recrystalization, interface trap states, etc. of the irradiated samples have significant effect on device performance [6,7]. Zhang et al. [8] reported that TiO_2 being a high k gate dielectric can be a good alternative of SiO_2 in radiation environments. In radiation environments, the density of Ti^{3+} ions increases over that of Ti^{4+} ions at the TiO_2/Si interface. This valence variation is beneficial to the stability in TiO_2/Si structures [8]. High k metal oxides possess narrow band gaps and high scattering cross sections whereas Al_2O_3 has a wide band gap and low scattering cross section as compared to other oxides [9]. In addition to this, Al_2O_3 has high band offsets to Silicon providing low leakage current. In view of this, a multilayer of TiO_2 and Al_2O_3 may be a good substitute for SiO_2 for fabricating radiation hardened MOS devices [10,11].

In the present work, $Al/Al_2O_3/TiO_2/n$-Si MOS capacitors were obtained using r.f. reactive magnetron sputtering. The capacitors were irradiated with 6 MeV electrons of 10, 20, and 30 kGy doses. The dielectric losses of the virgin and the irradiated samples were compared. The device parameters have been estimated using C–V and G/ω–V curves. The leakage current mechanism has been explained using the $\ln|J|$ versus $E^{1/2}$curves. D_{it} value of irradiated $Al/Al_2O_3/TiO_2/n$-Si MOS capacitor has been compared with reported data [7].

2. Experimental details

MOS structures of $Al/Al_2O_3/TiO_2/n$-Si were prepared using r.f. reactive magnetron sputtering. The details of the deposition

* Corresponding author. Present address: Department of Physics and Astronomy, University of California, Los Angeles, CA 90095, USA.
E-mail addresses: skm@physics.ucla.edu, skmahapatra@bitmesra.ac.in (S.K. Mahapatra).
[1] Department of Mechanical and Aerospace Engineering, University of California, Los Angeles, CA 90095, USA.

0168-583X/$ - see front matter © 2012 Elsevier B.V. All rights reserved.
http://dx.doi.org/10.1016/j.nimb.2012.04.014

system have been reported elsewhere [12]. *n*-Type silicon of size 10 mm × 10 mm were used as substrates after cleaning initially with dilute HF acid, deionized water and dried at room temperature prior to deposition. Both Ti (99.99%) and Al (99.99%) targets were sputter cleaned by pure (99.9%) Argon gas before deposition.

To achieve the MOS structure of Al/Al_2O_3/TiO_2/*n*-Si, multilayers of TiO_2, Al_2O_3 and Al were successfully deposited on the *n*-Si substrate. Three types of MOS structures (Al/Al_2O_3/TiO_2/*n*-Si) were obtained by variation in deposition time from 8 to 12 min in steps of 2 min for TiO_2 and 4–8 min for Al_2O_3. Each layer was deposited at O_2:Ar gas ratio of 50:50 sccm, working pressure of $\sim 5 \times 10^{-2}$ mbar and r.f. power of 100 W one by one without breaking the chamber pressure and by simple rotation of the sample holder. A thin film of metallic aluminum of thickness 275 nm was then deposited on the Al_2O_3/TiO_2 coatings, by a deposition time of 7 min. A deposition time of 6 min for $Al_2O_3$and 10 min for TiO_2 provided a total stack thickness of 100 nm for the Al_2O_3/TiO_2 heterostructure. The results also confirmed that the film uniformity and crystallinity remain undistorted for the deposited films of 100 nm thickness. In a multilayer sample, during the switching time of TiO_2 deposition to Al_2O_3 deposition, the existing Ti vapors in the chamber may cause interdiffusion of layers (Ti and Al) along with the deposition of Al_2O_3. The sequential film growth process is followed by solid vapor transformation through heat released to substrate undergoing heterogeneous nucleation [13].

All these laboratory made Al/Al_2O_3/TiO_2/*n*-Si MOS capacitors were characterized by (i) Ellipsometer (Nano – View Inc., Korea; SEMG1000-VIS) for the measurement of layer thickness (ii) SIMS (Model: Hiden, UK) for in depth elemental analysis (iii) GIXRD (Model: PAN analytical X′ Pertpro 3040/60) for measurement of crystallographic structure (iv) *C–V*, G/ω–*V* and Tan δ–*V* (HP4284 LCR Meter) for the estimation of device parameters (v) current–voltage (2410 Keithley Source meter) measurement for leakage current study.

A few of the characterized MOS capacitors were divided into four groups, each consisting of three capacitors. The first group of non-radiated MOS capacitors was treated as virgin. Second, third and fourth group of capacitors were irradiated with 6 MeV electrons with different electron doses. The 6 MeV electron beam of pulse width ~1.6 μs had diameter ~3 mm after exiting from the extraction window of the Microtron. The electron beam was therefore, scattered by a thin tungsten foil to cover the entire area (10×10 mm^2) of the capacitor. For irradiation, one capacitor at a time was mounted on the Faraday cup placed at a distance of ~150 mm away from the extraction port in air. The Faraday cup was connected to a current integrator for measuring the number of electrons falling on the capacitor. In this manner, each capacitor of the first group was irradiated with 6 MeV electrons to a dose of 10 kGy. Similarly, second and the third groups of capacitors were irradiated with 6 MeV electrons with doses of 20 and 30 kGy, respectively, at a constant dose rate of ~1 kGy per minute and then the electron irradiated capacitors were characterized and analyzed.

3. Basic theory

3.1. MeV energy electron irradiation effects

MeV electrons interact with materials by several mechanisms. When energetic electrons penetrate the target sample their energy gets transferred for ionization and excitation of the target atoms. Low-energy electrons can transfer only a few eV to the target atoms, which is not enough to displace atoms from their lattice sites. For high energy electron beam (~MeV), the target atom acquires enough kinetic energy to get displaced from its position in the atomic network [14]. The point defects such as vacancy–interstitial pairs disappear immediately after the impact of electron energy [15]. Due to "hot spot effect" extra heating may transfer the energy which reduces the point defect by creating new bond with another atom [14]. Some of the defects remain in the system or form more complicated defect structures after electron irradiation. In addition, the kinetic energy transferred to atomic arrangement through extra heating produce bond breaking, dangling bonds, defects, recrystalization and re-bonding [16].

3.2. Interfacial defect capacitance and interface trap density

The interfacial defects arise from the mismatch of crystal structure, nonstoichiometric cation or anion vacancies and interdiffusion of atoms known as dangling bonds at the interface. These dangling bonds produce defect states near the conduction and valence band edge. The value of interfacial defect and interfacial capacitance may change due to electron irradiation. The interfacial trap density (D_{it}), interfacial defect capacitance (C_{it}) and dose rate (D_r) are related through the following equations [17,18]:

$$C_{it}(f) = q.D_{it} \tag{1}$$

$$D_{it} = \kappa_g.f_y.D_r.t_{OX}.f_{it}, \tag{2}$$

where, κ_g represents the number of electron–hole (e–h) pairs produced per unit dose, f_y, the probability that an e–h pair escapes recombination, $t_{ox,}$ *the* oxide thickness, D_r, the radiation dose rate and f_{it}, the number of interface traps created per radiation-induced e–h pair. At the interface, dangling bonds are contributed by interface trap density (D_{it}). D_{it} is calculated by Hill–Coleman method using the following equation [19]:

$$D_{it} = \frac{2}{qA}\frac{\left(\frac{G_m}{\omega}\right)_{\max}}{\left(\left(\frac{G_m}{\omega}\right)_{\max}.C_{OX}\right)^2 + \left(1 - \frac{C_m}{C_{OX}}\right)^2}. \tag{3}$$

Generally, the oxide layer of MOS structure forms two types of interface layers, one with the top metal gate and other with the bottom Si substrate. In case of multilayer oxide in MOS structure, additional interface is generated in the multilayer. This type of interface growth depends on oxygen affinity to create bonds with the metal or Si at the interface. Generally, the bottom interface affects the Si channel mobility, while the defects at the metal–insulator interface cause Fermi level pinning, which affects the transistor current.

3.3. Conductivity

The radiation induced conductivity C_r and the dose rate D_r are related through the following expression [20]:

$$C_r = \varepsilon k D_r^n \tag{4}$$

where, k is a constant, $\varepsilon(\varepsilon_0\varepsilon_r)$ is the dielectric constant of the oxides and the exponent n is energy distribution of the radiation induced traps in the oxide layers. It implies that the conductivity C_r increases with increasing dose rate D_r. The conductivity in oxides is governed mostly by the mechanism of hopping charge carriers. The number of sites available for hopping increases with electron doses. This enhances the mobility of charge carriers throughout the MOS capacitor. The mobility of the electrons also depends on the crystal lattice, impurities, vacancies, defects of the materials, etc. The relation between the mobility and dose rate is [21]:

$$\mu = (const) D_r^{2\Delta - 1}, \tag{5}$$

where, Δ = exponent for dose rate. Trapped induced carriers generally increases with the increasing radiation dose.

3.4. Tan δ

Tan δ is the dissipation factor which depends on the dipoles of the dielectric material. The dielectric relaxation is governed by the following equation [22]:

$$\mathrm{Tan}\,\delta = \frac{2\pi f \tau_0 S_r}{1 + (2\pi f \tau_0)^2}, \tag{6}$$

where, S_r = relaxation strength, τ_o = relaxation time for dipole orientation, f = frequency of the applied electric field. The relationship, $\omega \cdot \tau_o \cdot T \sim 1$ is applicable to the dielectric loss peak.

3.5. Leakage current mechanism

Conduction in MOS device is controlled by several mechanisms. These are mainly, Schottky, Poole–Frenkel and Fowler–Nordheim emission mechanisms. In the present case, the possible mechanism has been considered to be Frenkel–Poole emission. The leakage current equation for Frenkel–Poole emission is given by the following expression [12],

$$J = J_0 \exp[(\beta_{PF} E^{1/2} - \phi_{PF})/K_B T], \tag{7}$$

where, ϕ is the barrier height, $J_0 = \sigma_0 E$ is the low-field current density, σ_0 is the low-field conductivity and β_{PF} is Frenkel–Poole emission coefficient given by,

$$\beta_{PF} = \left(\frac{e^3}{\pi \varepsilon_0 \varepsilon_{OX}}\right)^{1/2}. \tag{8}$$

4. Results and discussion

Fig. 1 shows the SIMS depth profiles for the sample of Al/Al_2O_3/TiO_2/*n*-Si. As seen in the figure, the measured oxide film (Al_2O_3/TiO_2) thickness is found to be in close agreement with the desired thickness of 100 nm. The thickness of the Al cap layer for all samples as measured through SIMS is of ~275 nm. As seen in Fig. 1, the small hump of Al is due to the Al_2O_3 layer and the peak of Ti appearing immediately after the Al hump clearly signifies the presence of TiO_2 interlayer. The figure also suggests that both oxygen and titanium have interdiffused into the substrate and silicon has largely diffused in the entire multilayer stack. The enhanced Al signal in Al_2O_3 interlayer is possibly due to the 'matrix effect' in SIMS.

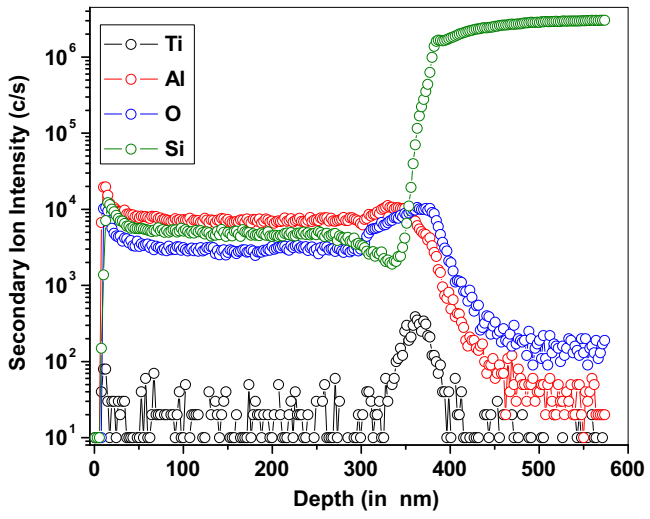

Fig. 1. SIMS depth profiles Al/Al_2O_3/TiO_2/*n*-Si structures.

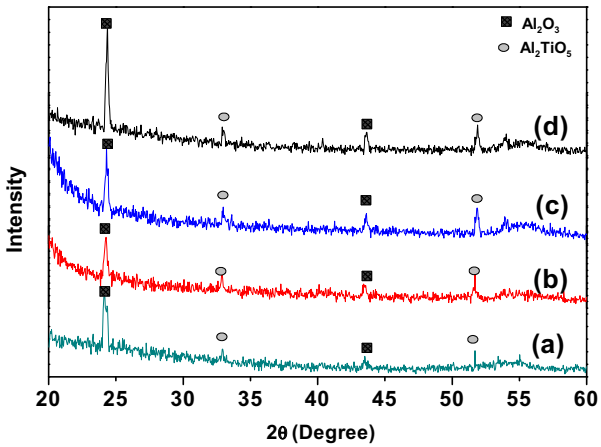

Fig. 2. GIXRD spectra of Al_2O_3/TiO_2 thin film with different electron radiation dose (a) zero (virgin), (b) 10 kGy, (c) 20 kGy, and (d) 30 kGy.

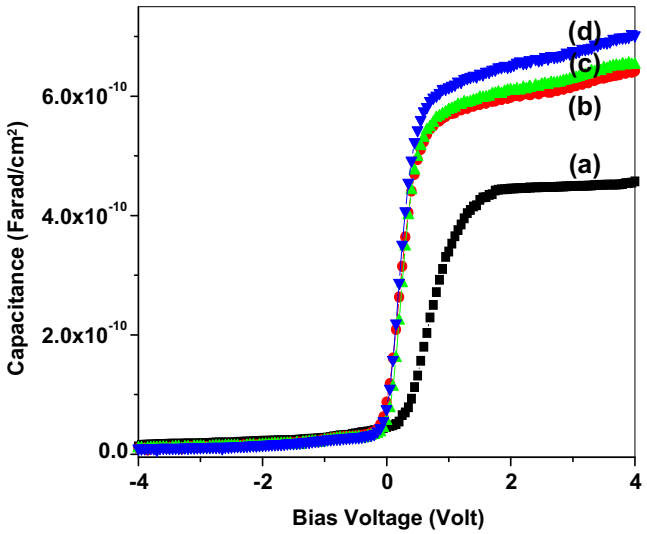

Fig. 3. *C–V* characteristics of Al/Al_2O_3/TiO_2/*n*-Si MOS capacitor with different electron radiation dose (a) zero (virgin), (b) 10 kGy, (c) 20 kGy, and (d) 30 kGy.

GIXRD spectra of Al_2O_3/TiO_2 irradiated with 6 MeV electrons at different dosesof (a) zero (virgin), (b) 10 kGy, (c) 20 kGy, and (d) 30 kGy are shown in Fig. 2. Fig. 2 shows peaks at $2\theta = 25.2°$, 33.99°, 44.12° and 54.49° corresponding to the planes (012) of Al_2O_3, (023) of Al_2TiO_5, (202) of Al_2O_3 and (044) of Al_2TiO_5, respectively. Al_2TiO_5 peaks show significant intermixing of TiO_2 and Al_2O_3 in the Al_2O_3/TiO_2 film. Generally, magnetron sputter deposited multilayer thin film experiences back sputtering process which leads to interfacial diffusion of atoms but not leading to any substantial increase in crystal structure development [23]. Thus the film is amorphous but interfacial interdiffusion occurs at the time of deposition and Al_2TiO_5 forms at the interface of TiO_2 and Al_2O_3 layer. Furthermore, the peak intensity of Al_2TiO_5 increases with increasing electron dose. The increase in intensity may be due to the proper intermixing and recrystalization at the interface induced by energetic electrons. The 6 MeV electrons transfer the energy to the lattice point causing local heating and recrystalization in the sample.

Fig. 3showsthe *C–V* characteristics of Al/Al_2O_3/TiO_2/*n*-Si samples irradiated with 6 MeV (at 500 kHz) electrons at different dosesof (a) zero (virgin), (b) 10 kGy, (c) 20 kGy and (d) 30 kGy. It

shows that the capacitance at accumulation region increases with increasing electron dose. Eqs. (1) and (2) show that interfacial capacitance (C_{it}) and interfacial trap density (D_{it}) are proportional to dose rate (D_r). The observed results show enhancement of the capacitance in the irradiated samples with the increase in the electron dose rate. A parallel shift of the depletion region was observed in all the irradiated samples towards the negative voltage side with respect to the electron dose rate. The capacitance slowly increases with the bias voltage compared to the virgin sample. It may be due to enrichment of interface defects and charge trapping at the interfaces, which increases the creation of effective oxide charges after electron irradiation. The shifting of depletion region towards the negative bias might be due to hole trapping at the vacancy sites of oxide layer [24].

Flat band capacitance (C_{FB}) was calculated using the equation:

$$C_{FB} = \frac{(C_{OX}.C_{SFB})}{(C_{OX} + C_{SFB})}, \tag{9}$$

where, C_{SFB} is the depletion layer capacitance, C_{ox} is maximum value of the capacitance in C–V plot and C_{FB} is the corresponding voltage for Flat band voltage (V_{FB}). Fig. 4 shows significant changes in flat band voltage and total charge density due to electron irradiation. It shows that flat band voltage decreases with increase of electron dose. The Ti^{4+} get transferred to Ti^{3+} states in TiO_2 to compensate the charge state due to the irradiation, therefore, generating the negative O^- charges in the sample [25]. These extra charges cause decrease of the flat band voltage ΔV_{FB}. The higher electron dose induces excess electron–hole pairs creating more positive charge in the transition layer. This causes shifting of the depletion region towards negative voltage.

Total Charge Density (Q_{SS}) was calculated using the formula:

$$Q_{SS} = \frac{C_{OX}}{A}|\phi_{MS} - V_{FB}|, \tag{10}$$

where, A = area of the sample and Φ_{MS} is metal–semiconductor work function. Q_{SS} increases initially and then decreases with electron dose which is shown in Fig. 4. At lower dose, the oxide charge increases with respect to the initial fixed charge in the oxide layer of the irradiated sample. At higher dose the increased positive oxide charges get attached to the oxygen-vacancies and dangling bonds which generate low charge density [26].

Fig. 5 shows the G/ω–V characteristics of Al/Al_2O_3/TiO_2/n-Si samples irradiated with 6 MeV (500 kHz) electrons at different

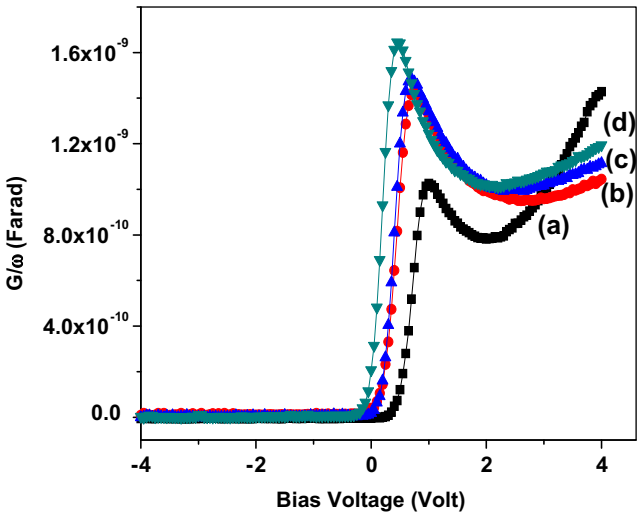

Fig. 5. G/ω–V characteristics of Al/Al_2O_3/TiO_2/n-Si MOS capacitor with different electron radiation dose (a) zero (virgin), (b) 10 kGy, (c) 20 kGy, and (d) 30 kGy.

dosesof (a) zero (virgin), (b) 10 kGy, (c) 20 kGy, and (d) 30 kGy. It shows that the conductance increases with increasing electron dose from 10 to 30 kGy at the accumulation region. The result is well in agreement with the governing Eq. (4). Furthermore, a peak in Al/Al_2O_3/TiO_2/n-Si sample confirms the presence of interface states getting activated due to 500 kHz frequency.

The formation of more interface states may be due to extra unsaturated bond formation in Al/Al_2O_3/TiO_2/n-Si sample on account of intermixing of two different oxide materials. The conductivity in oxides is governed mostly by the hopping mechanism. Hopping charge carrier increases with increasing electron irradiation dose as phase transitions of the oxide layers from amorphous to crystalline occur due to the electron radiation [27]. Eq. (5) is well in agreement with our experimental data. The variations in dangling bonds, recrystalization and defects due to electron dose may vary the conductance properties of the MOS structure. The interface trap density D_{it} was estimated by Hill–Coleman method using Eq. (3).

Fig. 6shows the D_{it} value of Al/Al_2O_3/TiO_2/n-Si samples irradiated with 6 MeV electrons at different dose rates of (a) zero (virgin), (b) 10 kGy, (c) 20 kGy, and (d) 30 kGy. It shows that D_{it}

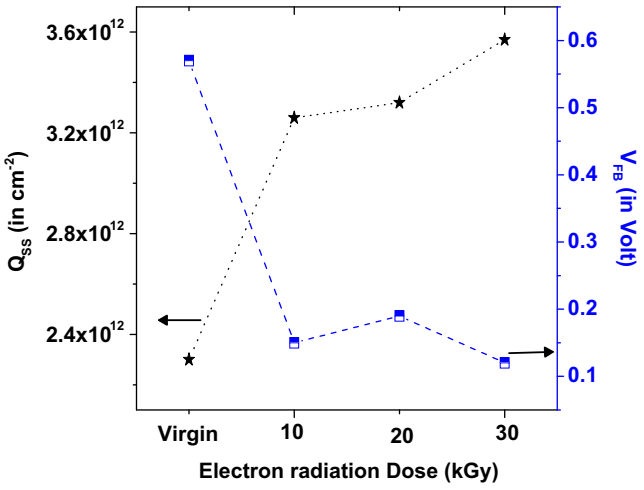

Fig. 4. Flatband voltage (V_{FB}) and surface charge density (Q_{SS}) of Al/Al_2O_3/TiO_2/n-Si MOS capacitor with different electron radiation dose (a) zero (virgin), (b) 10 kGy, (c) 20 kGy, and (d) 30 kGy.

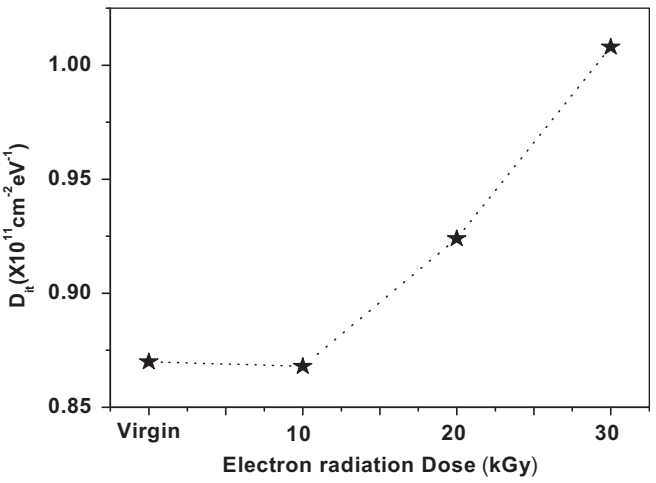

Fig. 6. D_{it} of Al/Al_2O_3/TiO_2/n-Si MOS capacitor with different electron radiation dose (a) zero (virgin), (b) 10 kGy, (c) 20 kGy, and (d) 30 kGy.

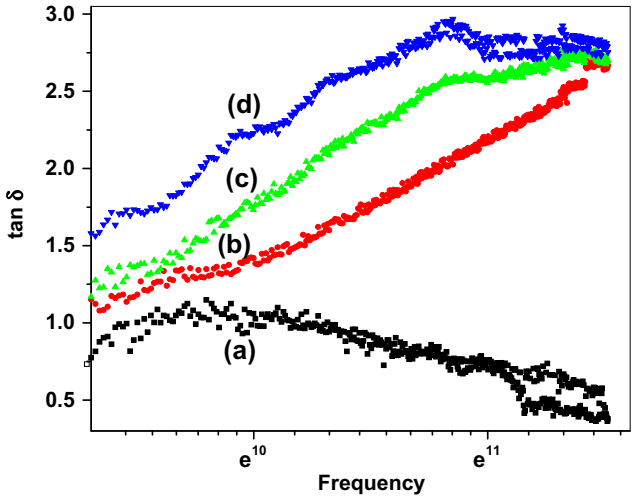

Fig. 7. Tan δ of Al/Al_2O_3/TiO_2/*n*-Si MOS capacitor with different electron radiation dose (a) zero (virgin), (b) 10 kGy, (c) 20 kGy, and (d) 30 kGy.

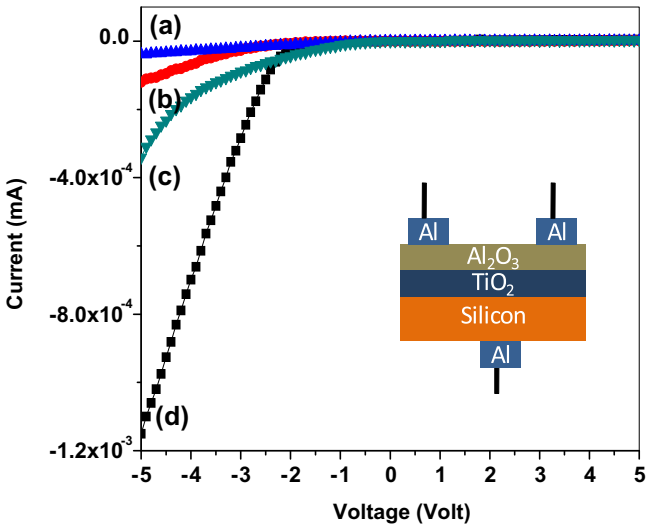

Fig. 8. *I–V* characteristics of Al/Al_2O_3/TiO_2/*n*-Si MOS capacitor by varying different electron radiation dose (a) zero (virgin), (b) 10 kGy, (c) 20 kGy, and (d) 30 kGy and schematic of its measurement setup is shown in inset.

increases with increasing electron irradiation dose. Generally, D_{it} depends on the dangling bonds existing at the interface. These variations were expected because 6 MeV is sufficient to break Si–Si, Al–O or Ti–O bond and create dangling bonds at the interface. García et al. [7] reported that interface trap density (D_{it}) of ALD deposited HfO_2/SiO_2 is $\sim 10^{12}$ cm^{-2} eV^{-1} which is higher than our observed value($\sim 10^{11}$ cm^{-2} eV^{-1}).

Fig. 7 shows Tan δ versus frequency plot in the range of 1 Hz to 100 kHz for Al/Al_2O_3/TiO_2/*n*-Si samples irradiated with 6 MeV electrons at different dosesof (a) zero (virgin), (b) 10 kGy, (c) 20 kGy, and (d) 30 kGy. Eq. (6) shows that Tan δ depends on dielectric strength S_r. In addition to this, S_r depends on the concentration of the dipoles and the square of their dipole moments. When high energetic electron beam strikes the target then more number of dangling bonds are formed subsequently more dipoles are also produced. Due to this Tan δ increase with increasing electron irradiation. In each spectrum of irradiated samples, the relaxation loss peak is broader and it depends on the dielectric relaxation period, τ. This broad peak is due to the overlapping of large number of different relaxation periods of the dipoles. The peak in the spectrum shifts with increase in electron dose. The appearance of a peak in Tan δ versus log *f* curve is due to matching of hopping frequency with frequency of external electric field. This is popularly known as interfacial polarization as established by Koops and Maxwell–Wagner model [28–30]. Furthermore, the shift in the relaxation loss peak indicates that relaxation time period (τ_0) for dipole orientation changes with the electron dose. The observed peak shifting in the spectrum is due to the variations in dangling bonds which is more effective for the interfacial polarization.

Fig. 8 shows the leakage current (*I*) versus voltage (*V*) for the samples Al/Al_2O_3/TiO_2/*n*-Si samples irradiated with 6 MeV electrons with different doses. In the negative bias condition, the current variations are more prominent after −1 V for all the four samples. After that, the current changes rapidly with increasing bias voltage. In Fig. 8(a) virgin sample shows that the variation in current is very less up to −4 V, after that the current increases rapidly and reaches the maximum current of -3.5×10^{-5} mA at −5 Volt. Fig. 8(b) shows that the current for 10 kGy dose sample is very less up to −3 V and after that the current increases rapidly and reaches the maximum current of -1.17×10^{-4} mA at −5 V. Fig. 8(c) shows that the current for 20 kGy dose sample is -3.12×10^{-5} mA at −1.5 V, after that the current increases and reaches the maximum value of -3.4×10^{-4} mA at −5 V. Similarly, Fig. 8(d) for 30 kGy dose samples a current of -1.13×10^{-3} mA is observed at −5 V which is higher compared to the other cases. Generally, the interface between Si and TiO_2 layer affects the Si channel mobility. The defects at the metal (Al)–insulator (Al_2O_3) interface cause the Fermi level pinning, which affects the changes in the transistor drive current. Fig. 8 shows no identifiable trend in the behavior of the leakage current with irradiation dose, which implies that the excited traps have only a minor effect on current. However, there is a significant change in threshold voltage for leakage current. The variation in leakage current may be due to the creation of dangling bonds through electron irradiation. For higher doses, some radiation-induced superfluous titanium generates extra energy states to the Si substrate [31]. These extra energy states exchange electrons with the Fermi level which contributes the extra current.

To understand the leakage current mechanism, we plotted ln $|J| - \sqrt{E}$ for Al/Al_2O_3/TiO_2/*n*-Si samples irradiated with 6 MeV electrons at different doses of (a) zero (virgin), (b) 10, (c) 20, and (d) 30 kGy as shown in Fig. 9. *J–V* plots were fitted to ln$J - \sqrt{E}$ plots

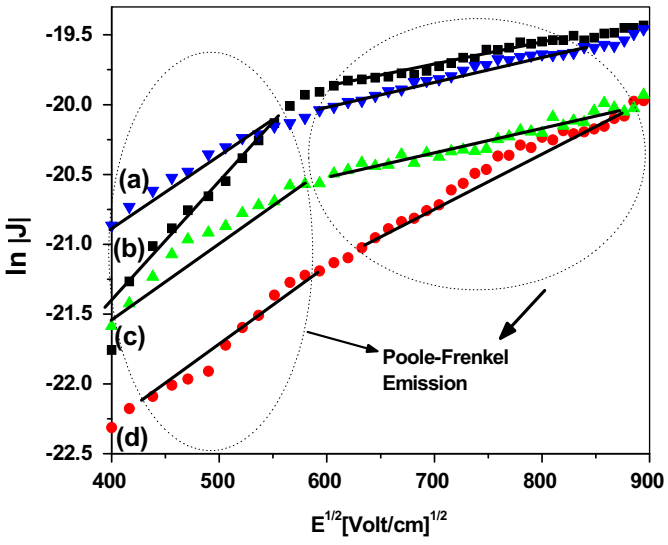

Fig. 9. Conduction mechanism fitting of Al/Al_2O_3/TiO_2/*n*-Si MOS capacitor by varying different electron radiation dose (a) zero (virgin), (b) 10 kGy, (c) 20 kGy, and (d) 30 kGy.

to explain the leakage current mechanism through Eq. (7). The figure shows that the behavior of $\ln|J|$ versus $\sqrt{E}$ is linear in nature. The slopes were obtained and used for estimating the experimental "β_{PF}" values. The experimental values of β_{PF} were compared with the theoretical values. The comparison shows that the leakage current of all virgin as well as irradiated MOS capacitors are due to Frenkel–Poole type conduction mechanism.

The possible mechanism of leakage current has been explained through: Frenkel–Poole emission. Frenkel–Poole emission is a trap assisted mechanism [32]. The trap densities in the oxide are seriously influenced by the Frenkel–Poole conduction. In our case, the oxide thickness is ~100 nm, which may be responsible for Frenkel–Poole mechanism in lower as well as higher electric fields. More the interface state and oxide defects, the more are the Frenkel–Poole emission induced leakage current. At lower applied fields, the electrons do not possess enough energy to overcome the potential barrier. The electrons tunnel through the barrier and get transported through the traps in the band gap of the insulator [33]. The trap assisted conduction is frequently arises at lower fields. At higher fields, barrier height gets reduced by the combined effect of the image field and the coulomb field. Positively charged trap levels eases the conduction process through conduction band. In this way, the linear behavior of conduction would be eliminated after an electron irradiation which is useful. Therefore, conduction mechanism could be controlled through modifications of interfaces by electron beam irradiation.

5. Conclusion

$Al/Al_2O_3/TiO_2/n$-Si MOS capacitors were prepared and irradiated with 6 MeV electrons with three different doses. Variations in the electrical parameters such as leakage current, conductance, flat-band voltage, interface trap density, and Tan δ of the MOS capacitor with the different electron doses were studied. It was observed that the 6 MeV electron beam caused variations in crystallinity, defects and dangling bonds at the interface, which eventually results in the variation of electrical properties. The outcomes indicate that the electrical parameters of such MOS capacitors may be customized by energetic electron beam irradiation.

Acknowledgement

The authors gratefully acknowledge the financial support received from BRNS, DAE, Mumbai, India.

References

[1] D. Binder, E.C. Smith, A.B. Holman, IEEE Trans. Nucl. Sci. NS-22 (1975) 2675–2680.
[2] F.A.S. Soliman, A.S.S. Al-Kabbani, K.A.A. Sharshar, M.S.I. Rageh, Appl. Radiat. Isot. 46 (5) (1995) 355–361.
[3] K.H. Zaininger, A.G. Holmes-Siedle, RCA Rev. 28 (1967) 208–240.
[4] P.F. Schmidt, M.J. Rand, J.P. Mitchell, J.D. Ashner, IEEE Trans. Nucl. Sci. Ns-16 (1969) 211–219.
[5] P.S. Winokur, J.R. Schank, P.J. Mcwhorter, P.V. Dressendorfer, D.C. Turpin, IEEE Trans. Nucl. Sci. Ns-31 (1984) 1453.
[6] M. Badila, Ph. Godignon, J. Millan, S. Berberich, G. Brezeanu, Microelectron. Reliab. 41 (2001) 1015–1018.
[7] H. García, S. Dueñas, H. Castán, A. Gómez, L. Bailón, R. Barquero, K. Kukli, M. Ritala, M. Leskelä, J. Vac. Sci. Technol. B 271 (2009) 416–420.
[8] J.D. Zhang, S. Fung, L.-B. Lin, Z.-J. Liao, Surf. Coat. Technol. 158–159 (2002) 238–241.
[9] V. Mikhelashvili, P. Thangadurai, W.D. Kaplan, G. Eisenstein, Microelectron. Eng. 87 (2010) 1728–1734.
[10] A.P. Alekhin, A.A. Chouprik, S.A. Gudkova, A. Markeev, M. Yu YuLebedinskii, Yu.A. Matveyev, A.V. Zenkevich, J. Vac. Sci. Technol. B 29 (2011) 01A302.
[11] O. Pakama, N. Serin, T. Serin, S. Altindal, J. Phys. D.: Appl. Phys. 41 (2008) 215103.
[12] P. Laha, A.B. Panda, S. Dahiwale, K. Date, K.R. Patil, P.K. Barhai, A.K. Das, I. Banerjee, S.K. Mahapatra, Thin Solid Films 519 (2010) 1530–1535.
[13] C. Merckling, M. El-Kazzi, L. Becerra, L. Largeau, G. Patriarche, G. Saint-Girons, G. Hollinger, Microelectron. Eng. 84 (2007) 2243–2246.
[14] J. Frantz, J. Tarus, K. Nordlund, J. Keinonen, Phys. Rev. B 64 (2001) 125313.
[15] Y. Ohno, Y. Kawai, S. Takeda, Phys. Rev. B 594 (15) (1999) 2694–2699.
[16] W.D. Callister Jr., G. Rethwisch David, R. Balasubramanium, Materials Science and Engineering, Wiley India (P) Ltd., 2009.
[17] C. Cheng-Wei, A. George, A. Fitzgerald Eugene, J. Appl. Phys. 109 (2011) 023714.
[18] H. Scofield John, M. Trawick, P. Klimecky, D.M. Fleetwood, App. Phys. Lett. 58 (1991).
[19] W.A. Hill, C.C. Coleman, Solid-State Electron. 23 (9) (1980) 987.
[20] S.K. Mahapatra, S.D. Dhole, V.N. Bhoraskar, G. RajuGorur, J. App. Phys. 100 (2006).
[21] B. Gross, G.M. Sesslerand, J.E. West, J. Appl. Phys. 56 (1974) 2333.
[22] P.S. Alegaonkar, V.N. Bhoraskar, P. Balaya, P.S. Goyal, Appl. Phys. Lett. 80 (4) (2002) 28.
[23] C. Imawan, H. Steffes, F. Solzbacher, E. Obermeier, Sens. Actuators B 78 (2011) 119–125.
[24] E.F. Belgin, R. Turan, S.T. Shishiyanu, Y. Ercan, Nucl. Instr. Meth. B 268 (2010) 482–1485.
[25] J.D. Zhang, S. Fung, L. Li-Bin, L. Zhi-Jun, Surf. Coat. Technol. 158–159 (2002) 238–241.
[26] P. Thangadurai, W.D. Kaplan, V. Mikhelashvili, G. Eisenstein, Microelectron. Reliab. 49 (2009) 716–720.
[27] K. Siraj, M. Khaleeq-ur-Rahman, M.S. Rafique, T. Nawaz, Nucl. Instr. Meth. B 269 (1) (2011) 53–56.
[28] J.C. Maxwell, A Treatise on Electricity and Magnetism, Dover, New York, 1891.
[29] K.W. Wagner, Ann. Phys. 40 (1913) 817.
[30] C.G. Koops, Phys. Rev. 83 (1951) 121.
[31] C. Liu, D. Wu, L. Zhao, Z. Liao, Nucl. Instr. Meth. B 268 (9) (2010) 1446–1449.
[32] A.A. Dakhel, Cryst. Res. Technol. 3811 (2003) 968–973.
[33] A.M. Roy, J.Y. Jason Lin, K.C. Saraswat, IEEE Electron Device Lett. 31 (10) (2010) 1077–1079.